

Theory of bound-state coherences generated and probed by optical attosecond pulsesWei-Chao Jiang^{1,2}, Xiao-Min Tong³, Renate Pazourek², Stefan Nagele², and Joachim Burgdörfer²¹*College of Physics and Optoelectronic Engineering, Shenzhen University, Shenzhen 518060, China*²*Institute for Theoretical Physics, Vienna University of Technology, Wiedner Hauptstraße 8-10, A-1040 Vienna, Austria, European Union*³*Center for Computational Sciences, University of Tsukuba, Tsukuba 305-8577, Japan*

(Received 27 November 2019; accepted 29 April 2020; published 28 May 2020)

We investigate the excitation and probing of electronic coherences in atoms by a sequence of optical attosecond pulses. Wave packets representing the coherent superposition of bound states in atoms are generated by a strong optical attosecond pulse. Amplitudes and phases of induced coherences can be retrieved from quantum beats in the radiative emission signal induced by a time-delayed weaker optical attosecond probe pulse. Such an attosecond-pump attosecond-probe scenario promises access to the excitation amplitudes and the off-diagonal elements of the density matrix generated by strong-field multiphoton processes. We illustrate this attosecond quantum beat spectroscopy with simulations for atomic hydrogen.

DOI: [10.1103/PhysRevA.101.053435](https://doi.org/10.1103/PhysRevA.101.053435)**I. INTRODUCTION**

Electromagnetic pulses with durations on the attosecond scale have opened up novel opportunities to monitor and steer electronic dynamics on its natural timescale. A large variety of approaches have been developed that allow us to temporally resolve electronic motion in atoms, molecules, and solids [1–6]. They include the attosecond streak camera [7,8], the interferometric method using reconstruction of attosecond beating by interference of two-photon transitions (RABBITT) [9,10], quantum-state holography [11,12], and attosecond transient absorption [13,14]. Most of the methods employed to date involve a weak extended (EUV) or extreme ultraviolet (XUV) attosecond pulse with photon energies ranging from 20 to 100 eV inducing one-photon transitions in the perturbative regime and a phase-controlled strong near-infrared (NIR) or mid-infrared (MIR) pulse generating multiphoton or strong-field processes. Accordingly, either the formation of the wave packet or its time evolution involves ionization, resulting in dephasing and decoherence of such an open quantum system.

An alternative interferometric method giving access to time-resolved information on bound-state dynamics is quantum-beat spectroscopy (QBS). It exploits the fact that the same final state can be reached by different pathways whose presence can be monitored in a time-resolved manner. QBS has a long history going back (at least) to beam-foil spectroscopy in the early 70s [15–18]. Fast atomic or ionic species were impulsively and coherently excited near the exit surface after traversing self-supporting thin carbon foils. Quantum beats were monitored in the time-resolved down-stream photon emission from fast projectiles. Time resolution was severely limited by the spatial resolution of the down-stream detection. Accordingly, beats on the nanosecond (or GHz) scale such as fine-structure quantum beats in light ions [18,19] and Lamb shift s - p coherence beats in hydrogenic systems

[20,21] could be resolved. More recently, using short laser pulses in a pump-probe setting, quantum-beat spectroscopy has become a key tool of femtochemistry for exploring vibrational dynamics of molecules [22,23]. Bound-state beats have been also mapped onto the ionization signal [24,25]. Following up on earlier work employing high-harmonic radiation [26,27], very recently, attosecond quantum beats of Rydberg wave packets in helium generated by synchrotron radiation have been demonstrated [28].

The recent breakthrough in synthesizing intense optical attosecond (OAS) pulses [29] resembling half-cycle pulses with an effective temporal width below one femtosecond [Fig. 1(a)] and a spectral distribution extending from ≈ 1 eV to about ≈ 4 eV [Fig. 1(b)] has allowed us to impulsively generate electronic bound-state wave packets in atoms involving electronic intershell coherences without strong coupling to ionization channels. With a time-delayed weaker optical attosecond pulse as a probe, the electronic wave packet motion can be mapped onto a quantum beat signal in photon emission from the excited states. We theoretically explore the observation of the coherences between electronically excited states generated by strong-field multiphoton excitation. We analyze the emerging quantum beat spectra in terms of the Liouville equation for the reduced density matrix which provides the natural framework for the description of partially coherent ensembles in the presence of inhomogeneous spatial distributions and temporal fluctuations in the driving and probing fields. We show that the excitation amplitudes, or, more generally, off-diagonal elements of the density matrix, strongly depend on the strength of the optical attosecond pulse, providing novel insights into the nonlinear atomic response on ultrafast timescales. Proof-of-principle simulations for hydrogen illustrate the opportunities and challenges of such an approach. An experimental realization involving rare-gas atoms is expected [30]. Atomic units are used unless stated otherwise.

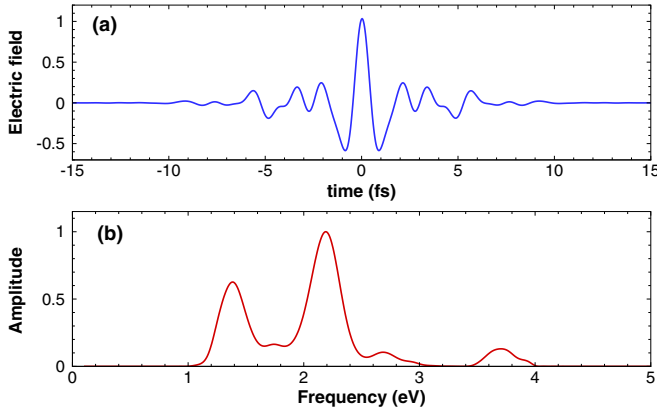


FIG. 1. (a) Temporal and (b) spectral profile of a typical optical attosecond (OAS) pulse (see Ref. [29]). (A Gaussian window function with width of 10 fs has been applied to remove pre- and postpulse tails).

II. THE OPTICAL ATTOSECOND PUMP-PROBE SCENARIO FOR BOUND-STATE PATH INTERFERENCES

Although the role of excited states is often neglected in the standard model for traditional high-order harmonic generation (HHG) [31–33], coherent XUV or EUV emission from the bound states, usually referred to as XUV free-induction decay (XFID) has recently received increased attention [34–37]. These coherent excited bound states can result from one-photon absorption [34,35], multiphoton absorption [36,37], or frustrated tunnel ionization [38]. A recent experiment indicates that XFID emission from excited bound states can be even stronger than the traditional HHG emission [38].

In the present study, we use the strong broad-band OAS pulse, referred in the following as the pump pulse (Fig. 1), to coherently excite a large number of excited atomic states with different principal (n) and angular momentum (ℓ) quantum numbers (Fig. 2). In hydrogen, the excitation gap to the lowest excited state ($1s \rightarrow 2p$) is $\Delta = 10.20$ eV, requiring, to lowest perturbative order, a three-photon absorption process for the strong OAS pump pulse. Through different orders of multiphoton processes that can be driven by the strong pump OAS pulse, states of different parity and a broad range of angular momenta can be accessed, opening a multitude of pathways for quantum interference. The large spectral width of the near half-cycle OAS pulse (Fig. 1) allows the impulsive buildup of coherently excited-state population, extending over several n levels of the atom. A second weaker probe OAS pulse, time-delayed by τ , couples these coherently excited states, e.g., $|i\rangle$ and $|j\rangle$, transferring the coherent population to another excited state $|e\rangle$. Hence, the state $|e\rangle$ is populated by a multitude of excited-state paths. Figure 2 depicts a representative sample of two of such paths. Each path to state $|e\rangle$ is generated by the excitation by the pump pulse and the (de)excitation by the probe pulse. Also, those paths can contribute for which either the pump or the probe pulse induces a direct transition from $|0\rangle$ to $|e\rangle$. In the following, we label each path leading to the state $|e\rangle$ by the “intermediate” state occupied in between pump and probe. The radiative decay of $|e\rangle$ to a lower-lying state (e.g., the $|1s\rangle$ state in the present case) carries the information

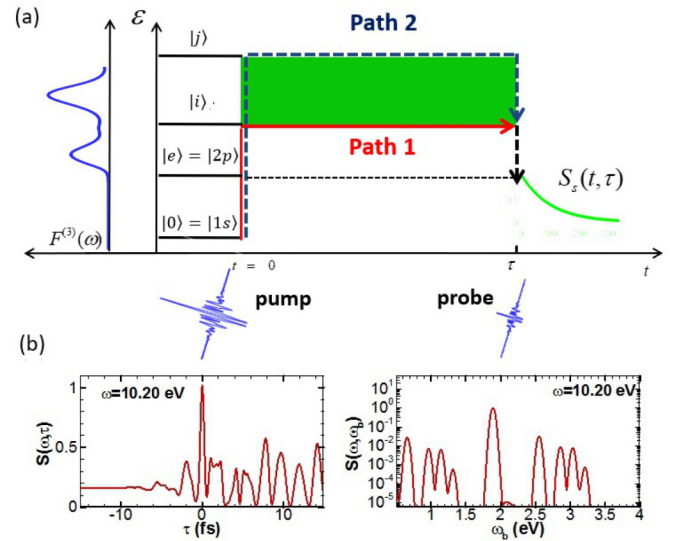


FIG. 2. (a) Quantum-beat spectroscopy and interfering pathways in hydrogen, schematically. The three-photon spectrum of the pump pulse $F^{(3)}(\omega) = \int d\omega_1 \int d\omega_2 F(\omega_1)F(\omega_2)F(\omega - \omega_1 - \omega_2)$ is shown on the left. At $t = 0$, impulsive excitation forms a coherent superposition of excited states $|k\rangle$ ($k = e, i, j, \dots$). A second OAS pulse at $t = \tau$ transfers the coherent population to the state $|e\rangle$. The time-resolved VUV signal from the radiative decay of $|e\rangle$ to the ground state $|0\rangle$, $S(t, \tau)$ [see Eq. (14)], features in addition to the exponential decay $\propto e^{-\Gamma t}$ quantum beats due to interfering pathways reaching the state $|e\rangle$, thereby providing information on impulsively induced coherences. The dynamical quantum beat phase is determined by the green shaded area, $|E_i - E_j|\tau$, in the energy-time diagram enclosed by different pathways. (b) The beat signal of the photon emission at energy of $|E_e - E_0|$ (left) and its frequency spectrum (right).

on the coherent multiphoton excitation and deexcitation of the states $|i\rangle$ and $|j\rangle$. Consequently, the photon emission signal S after the conclusion of the pump-probe pulse sequence will, in general, not only display an exponential decay [$\sim \exp(-\Gamma t)$] as a function of time t , but will feature oscillations (“quantum beats”) as a function of the time delay τ between pump and probe. From such quantum beats detailed information on the coherent wave packet dynamics, the energy spacing, and lifetimes of the states involved can be extracted.

In quantum beat spectroscopy, the energy eigenstates are the preferred basis (the “pointer states”) of coherences. In the present context coherences specifically refer to off-diagonal elements of the reduced density matrix in the basis of field-free energy eigenstates. Quantum beats give direct access to the magnitude and phase of such off-diagonal elements.

III. LIOUVILLE DESCRIPTION OF QUANTUM BEATS

We formulate the description of the time- (t) -differential photon emission signal $S(t, \tau)$ as a function of the delay τ between the attosecond pump and attosecond probe pulses and of the resulting QBS, $S(\omega, \tau)$, in terms of the time evolution of the (reduced) density matrix $\rho(t)$ [39] well suited for the description of, in general, partially coherent ensembles. The Liouville operator formulation [40–42] is particularly well adapted for describing QBS because the spectrum of the

Liouvillian directly yields the quantum beat spectrum. For clarity and readability, a brief summary of the Liouville space and superoperator notation is given in Appendix A.

The initial state of the system at time $t = 0$ taken in the following to be the ground state of the hydrogen atom with Hilbert space ket $|0\rangle = |1s\rangle$, just prior to the arrival of the OAS pump pulse $F_p(t)$, is represented by the initial density operator, the Liouville ket $|\rho(0)\rangle$. [Here and in the following, Liouville space kets, i.e., operators, are denoted by parentheses, $|a\rangle$, while Hilbert-space states are denoted by kets, $|a\rangle$]. In the present case,

$$|\rho(0)\rangle = |0\rangle\langle 0|, \quad (1)$$

corresponds to a pure state with Liouville norm $\langle \rho(0)|\rho(0)\rangle = \text{Tr}\rho^2 = \text{Tr}\rho = 1$. The strong ultrashort pump OAS of duration Δt_p transfers $|\rho(0)\rangle$ to

$$\begin{aligned} |\rho(\Delta t_p)\rangle &= \mathcal{U}(\Delta t_p)|\rho(0)\rangle \\ &= \hat{T} \exp\left(-i \int_0^{\Delta t_p} dt' \mathcal{L}(t')\right)|\rho(0)\rangle, \end{aligned} \quad (2)$$

where \mathcal{U} denotes the evolution operator in Liouville space, often referred to as evolution superoperator. \hat{T} denotes the time-ordering operator for the exponential function. The Hamiltonian entering \mathcal{L} [see Eq. (A9)] is given by

$$H(t) = H_0 + V(t), \quad (3)$$

consisting of the unperturbed atomic Hamiltonian H_0 and the coupling to the laser field $V(t)$. Equation (2) is explicitly given by

$$\begin{aligned} |\rho(\Delta t_p)\rangle &= \left\langle \hat{T} \exp\left(-i \int_0^{\Delta t_p} dt' H(t')\right) |0\rangle\langle 0| \right. \\ &\quad \left. \times \left[\hat{T} \exp\left(-i \int_0^{\Delta t_p} dt' H(t')\right) \right]^\dagger \right\rangle. \end{aligned} \quad (4)$$

An ensemble average over unobserved external degrees of freedom when applicable, e.g., in the present case the average over temporal fluctuations and spatial distributions of the field strength of the pulse over the focal volume [44–46] (“inhomogeneous line broadening”) is understood to be included in Eq. (4). In addition, the complex eigenvalues of H_0 result in homogeneous line broadening. Such ensemble averages will lead to, in general, partial loss of coherence $\langle \rho(t)|\rho(t)\rangle < 1$, even if the system was initially in a pure state. Both sources of decoherent dynamics are, thus, accounted for by Eq. (2).

The subsequent free evolution in between the pulses is accordingly given by

$$|\rho(t)\rangle = \exp[-i\mathcal{L}_{\text{free}}(t - \Delta t_p)]|\rho(\Delta t_p)\rangle. \quad (5)$$

In the field-free atomic energy eigenbasis, the matrix elements of the Liouville operator in Eq. (5),

$$[\mathcal{L}_{\text{free}}]_{j,j}^{i,i} = E_i - E_j - i \frac{\Gamma_i + \Gamma_j}{2}, \quad (6)$$

are diagonal (the pair of the upper and lower indices agree) and directly yield the quantum beat spectrum and the decay width of the coherences. Note that $\mathcal{L}_{\text{free}}$ is non-Hermitian due to the coupling of the atomic states to the vacuum fluctuations of the quantized radiation field leading to spontaneous

radiative decay with rates Γ_i treated in the Wigner-Weisskopf approximation [47,48].

The time-evolved density operator is exposed to the probe pulse $F_{\text{pr}}(t)$ of duration Δt_{pr} at $t = \tau$ (Fig. 2) resulting in another coherent redistribution of the wave packet. Accordingly, the Liouville ket at $t = \tau + \Delta t_{\text{pr}}$ reads

$$|\rho(\tau + \Delta t_{\text{pr}})\rangle = \mathcal{U}_{\text{pr}}(\Delta t_{\text{pr}})|\rho(\tau)\rangle, \quad (7)$$

with the evolution superoperator $\mathcal{U}_{\text{pr}}(\Delta t_{\text{pr}})$ constructed analogously to that for the pump pulse [Eq. (2)]. Finally, the subsequent free evolution up to the time of observation t is given by

$$|\rho(t)\rangle = \exp[-i\mathcal{L}_{\text{free}}(t - \tau - \Delta t_{\text{pr}})]|\rho(\tau + \Delta t_{\text{pr}})\rangle. \quad (8)$$

Time-resolved physical observables can now be extracted by projecting the Liouville ket onto the ket associated with the detection process. In the present case of OAS-pulse-induced vacuum ultraviolet (VUV) emission, two contributions need to be distinguished, the spontaneous emission from pulse-excited states (Fig. 2) taking place mostly after the pump-probe pulse sequence has passed and the stimulated emission by the strong-field driven wave packet during the intervals Δt_p and Δt_{pr} when the pulse is on [Eqs. (2) and (7)].

The stimulated strong-field photon emission is determined by the classical electric field generated by the field-driven accelerated charge cloud. Its far field is proportional to the Liouville ket,

$$\langle \mathbf{a} \cdot \hat{e} | \rho(t) \rangle = \text{Tr}(\mathbf{a} \cdot \hat{e} \rho(t)) = \langle \mathbf{a} \cdot \hat{e} \rangle_t, \quad (9)$$

where \hat{e} is the unit vector of the laser polarization and the acceleration operator \mathbf{a} is explicitly given by

$$\mathbf{a} = -\frac{\mathbf{r}}{r^3} - F(t)\hat{e}, \quad (10)$$

with the spectral frequency components

$$\langle \mathbf{a} \cdot \hat{e} \rangle_\omega = \int dt e^{i\omega t} \langle \mathbf{a} \cdot \hat{e} | \rho(t) \rangle. \quad (11)$$

The rate of induced (*i*) emission perpendicular to the polarization axis of the driving pulse is

$$S_i(\omega, \tau) = \frac{1}{2\pi c^3 \omega} |\langle \mathbf{a} \cdot \hat{e} \rangle_\omega|^2. \quad (12)$$

The corresponding angle-integrated emission rate is given by

$$S_i(\omega, \tau) = \frac{4}{3c^3 \omega} |\langle \mathbf{a} \cdot \hat{e} \rangle_\omega|^2. \quad (13)$$

The induced rate [Eqs. (12) and (13)] also depends implicitly on the pulse durations (Δt_p , Δt_{pr}) omitted in the following for simplicity.

For spontaneous (*s*) emission accompanied by a transition to the ground state (or, more generally, to a lower-lying final state $|f\rangle$) the spectrum is quasidiscrete with photon energies corresponding to transition energies $\bar{\omega}_k = E_i - E_f$. The emission signal is convoluted with a Gaussian spectral window function centered at $\bar{\omega}_k$ with an energy resolution $\Delta\omega_k$ corresponding to a time window of observation Δt . Quantum beats can also arise from the coherent superposition of different radiative decay paths (see Appendix B). In the present case we focus on the special case of field-free spontaneous emission

from a single excited state $|e\rangle$. The angle-integrated rate is accordingly given by [see Eqs. (B7) and (B8)]

$$S_s(\bar{\omega}_k, \tau, t) = \frac{4}{3c^3\bar{\omega}_k} |\langle f|\mathbf{a}|e\rangle|^2 \exp(-\Gamma_e t) \rho_{e,e}(\tau + \Delta t_{\text{pr}}). \quad (14)$$

The signal at photon energy $\bar{\omega}_k$ depends both on the time t elapsed subsequent to the preparation of the excited state, $\rho_{e,e}$, as well as on the pump-probe delay τ controlling the occupation of the excited state. The quantum beats analyzed in the following result from path interferences between pump and probe leading to oscillations in $\rho_{e,e}$ as a function of τ . Correspondingly, the time-integrated signal is given by

$$S_s(\omega, \tau) = \int_0^\infty dt S_s(\omega, t, \tau). \quad (15)$$

Finally, the quantum beat spectrum, the eigenvalue spectrum of the Liouvillian \mathcal{L} , follows then as the Fourier transform of the quantum beat signal with respect to the pulse delay τ ,

$$\tilde{S}(\omega, \omega_b) = \left| \int d\tau e^{i\omega_b \tau} S(\omega, \tau) \right|, \quad (16)$$

where

$$S(\omega, \tau) = S_i(\omega, \tau) + S_s(\omega, \tau). \quad (17)$$

It should be noted that, in the present scenario, contributions to S_i originate only from the two time intervals Δt_p and Δt_{pr} , while those to S_s originate (predominantly) from the time intervals during free evolution within which the driving field vanishes. Therefore, S_s strongly dominates over S_i . Equations (12) and (14) [see also Eq. (B7)] provide the complete description of the quantum beat signal accessible in the present OAS pump-probe scenario.

The key observables to be extracted include the distribution of beat frequencies [Eq. (6)]

$$\omega_b = E_i - E_j, \quad (18)$$

and the damping rates of the off-diagonal elements of the density matrix, i.e., of the coherences,

$$\Gamma_b = \frac{\Gamma_i + \Gamma_j}{2}. \quad (19)$$

The spectral width of the experimental signal may be, in addition, inhomogeneously broadened. It should be noted that the dynamical beat phase $\omega_b \tau$ acquired during the time delay τ [Eq. (16)] corresponds to the shaded area in the energy-time diagram (Fig. 2) enclosed by the interfering paths. Moreover, the phase shift θ for a given beat harmonic component, $\cos(\omega_b \tau + \theta)$, provides direct access to the relative phases $\Delta\phi$ of the transition matrix elements,

$$[\mathcal{Z}_p]_{i,0}^{j,0} = A_{i,0}^{j,0} \exp(-i\Delta\phi_{i,j}^0), \quad (20)$$

$$[\mathcal{Z}_{\text{pr}}]_{e,i}^{e,j} = B_{e,i}^{e,j} \exp(-i\Delta\phi_{i,j}^e), \quad (21)$$

with A, B being the moduli and

$$\Delta\phi_{i,j}^0 = \phi_{i,0} - \phi_{j,0}, \quad (22)$$

$$\Delta\phi_{i,j}^e = \phi_{e,i} - \phi_{e,j}, \quad (23)$$

being the relative phases for the transitions induced by the pump and probe. In terms of Eqs. (22) and (23), the beat phase shift is given by

$$\theta_{i,j} = \Delta\phi_{i,j}^0 + \Delta\phi_{i,j}^e. \quad (24)$$

The beat signal thus provides the full holographic information on the nonlinear electronic bound-state response to a strong attosecond-scale perturbation.

We simulate the light emission [Eq. (17)] and the quantum beat signal by calculating the time evolution of the density operator $\rho(t)$ from ensemble averages over numerical solutions of the time-dependent Schrödinger equation (TDSE) [49]. The ensemble extends over different realizations of the OAS pulse, examples of which will be given below. Since we solve the nonrelativistic TDSE, fine-structure and Lamb shift splittings are neglected and the ℓ degeneracy persists. The TDSE is solved by discretizing the radial wave function by the finite-element discrete variable representation (FEDVR) method [50–52], and the split-Lanczos algorithm is used to propagate the wave function in time. We take the experimentally measured OAS laser pulse in Ref. [29] to perform the calculations. A Gaussian window function with width of 10 fs is applied to the experimental OAS laser pulse to remove the pre- and postpulse tails. The TDSE results for the strong-field dynamics [Eqs. (2) and (7)] presented in the following are calculated in the velocity gauge [$V(t) = -i\mathbf{A}(t) \cdot \nabla$]. However, we have carefully checked for gauge invariance of the solution. The free evolution after the conclusion of the pulse determining the spontaneous emission is calculated analytically by employing the nonunitary evolution generated by the non-Hermitian Liouvillian [Eq. (6)] with analytically calculated eigenstates of H_0 . The resulting emission spectrum is convoluted with a (Gaussian) spectral window function corresponding to an energy resolution of $\Delta\omega_k = 0.1$ eV or a time window of observation $\Delta t \approx 30$ fs.

IV. DENSITY MATRIX AND QUANTUM BEATS FOR HYDROGEN

The starting point of the analysis is the VUV emission spectrum decomposed into the induced and spontaneous components [Eq. (17)] generated by the pump pulse only (Fig. 3). The induced emission displays a broad nonlinear subthreshold harmonic spectrum while the spontaneous emission features the characteristic line spectrum of the Lyman series. The latter results from the population of np states excited by the OAS pump pulse. Although here only p states significantly contribute to the spontaneous light emission spectrum due to the dipole selection rule, many degenerate ℓ states will contribute to the quantum beat signal as discussed below. The spontaneous emission signal strongly dominates over the induced signal. On the level of the strong single-atom response considered here the induced emission provides a significant contribution only in spectral regions far from the positions of the discrete lines (Fig. 3). The intensities of the spectral lines depend on the occupation probabilities of the emitting states given by the diagonal elements of the density operator $|\rho(t)\rangle$ in the energy eigenbasis and extend to dipole-forbidden states $\ell \neq 1$ (Fig. 4) reflecting the multiphoton excitation by the OAS pulse. The nonmonotonic increase and oscillations

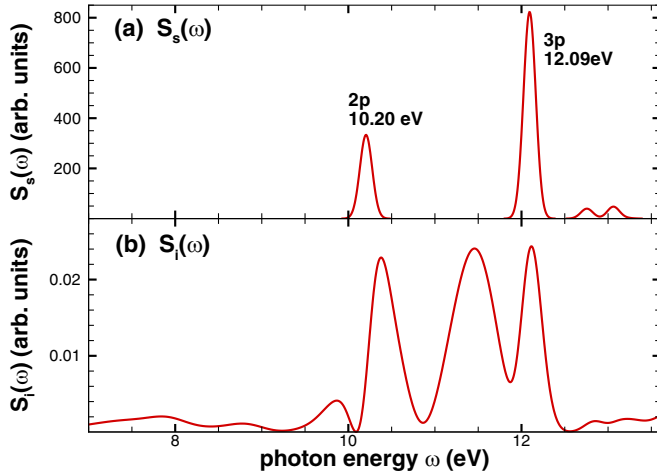


FIG. 3. Photon emission induced by the pump OAS pulse with peak intensity $7 \times 10^{13} \text{ W/cm}^2$: (a) spontaneous emission $S_s(\omega)$, (b) strong-field-induced signal $S_i(\omega)$ (note the different scales).

with the intensity of the pump pulse resembles Rabi flopping dynamics [53] and is the hallmark of strong-field driving.

Turning now to the pump-probe scenario, the rapid sub-cycle variation of the occupation probabilities as a function of time delay τ between pump and probe (Fig. 5) clearly indicates the attosecond-scale response to the OAS pulse. The strong population of the $|2p\rangle$ state at time delay $\tau = 0$ between the pump and the probe OAS pulses can be detected in the subsequent spontaneous photon emission from the $|2p\rangle$ state to the ground state, as shown in Fig. 6.

The quantum beats in the occupation probabilities (Fig. 5) are directly accessible in the subsequent photon emission. The attosecond coherence in bound-state excitation appears in the VUV emission signal recorded as a function of pump-probe delay τ (Fig. 6). Temporal oscillations of the emission signal from the low-lying excited states ($2p$, $3p$, ...) as a function of τ are clearly recognizable. They directly mirror the oscillations seen in Fig. 5.

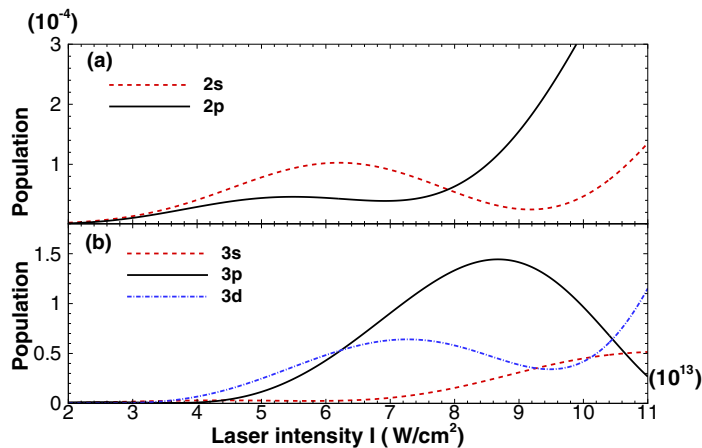


FIG. 4. The population of several excited states as a function of the intensity of the pump OAS pulse for (a) $n = 2$, (b) $n = 3$.

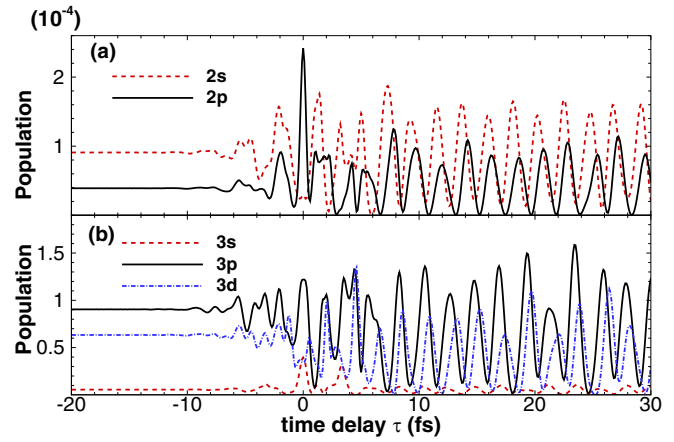


FIG. 5. The population of several excited states after the conclusion of the probe pulse as functions of the time delay τ . The peak intensity of the pump pulse is $I_p = 7 \times 10^{13} \text{ W/cm}^2$, and the peak intensity of the probe pulse is $I_{pr} = 2 \times 10^{12} \text{ W/cm}^2$; (a) $n = 2$, (b) $n = 3$.

The quantum beat pattern can be analyzed by Fourier analysis of the quantum beat signal [Eq. (16)]. The resulting quantum beat map (Fig. 7) provides detailed insights into the multitude of interfering excitation paths that become accessible by strong-field OAS pulses. Examples for different classes of path pairs contributing to the interference pattern are marked. For example, the population of the $2p$ state spontaneously decaying back to the ground state can be generated by a multiphoton excitation from the ground state by either the pump pulse at $t = 0$ or by the probe pulse at $t = \tau$. The

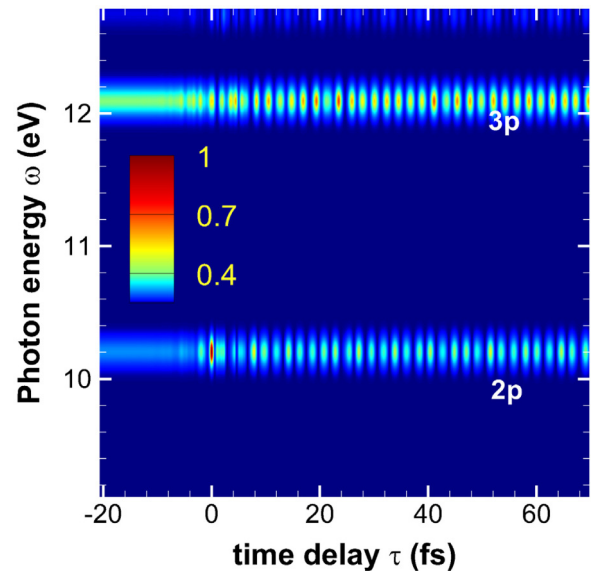


FIG. 6. The VUV emission spectrum normalized to the maximum as function of time delay τ between the OAS pump pulse ($I_p = 7 \times 10^{13} \text{ W/cm}^2$) and OAS probe pulse ($I_p = 2 \times 10^{12} \text{ W/cm}^2$). The emission lines back to the ground state are labeled by the emitting states from which the transition occurs. The spectrum is completely dominated by spontaneous emission. The induced component would appear only when a logarithmic rather than a linear color scale would be used.

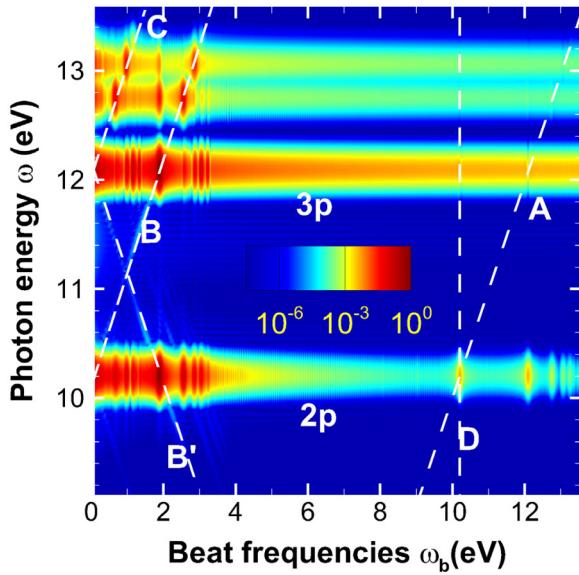


FIG. 7. Fourier quantum beat map normalized to the maximum as a function of the beat frequency in units of energy (eV) calculated by a Fourier transform of the time-delay resolved VUV emission spectrum (Fig. 6). Similar to Fig. 6, the horizontal emission lines back to the ground state are labeled by the emitting states ($2p$, $3p$) from which the transition occurs. Intersections of tilted lines A ($\omega = \omega_b$), B ($\omega = \omega_b + E_{n=2} - E_{1s}$), and C ($\omega = \omega_b + E_{n=3} - E_{1s}$) with the horizontal emission lines mark the contribution of different interfering pairs of paths (Fig. 2): pairs involving the emitting state and the ground state lie on line A, those with the emitting state and an $n = 2$ state lie on line B, those with the emitting state and an $n = 3$ state lie on line C. Note that intermediate nl states can have any angular momentum. The vertical line D ($\omega_b = E_{n=2} - E_{1s}$) marks the position of the interference contribution from the fixed path pair ($1s$, $2p$) of intermediate states to different emission lines with which the line intersects.

enclosed interference “area” [Fig. 2(a)] gives rise to a quantum beat peak at the frequency $\omega_b = E_{2p} - E_{1s} = 10.2$ eV, marked by the intersection of line A (the diagonal $\omega = \omega_b$) and the horizontal $2p$ emission line (Fig. 7). Likewise, the pump pulse can coherently excite $n = 2$ or $n = 3$ at $t = 0$. If now the probe pulse transfers the electron from $n = 2$ to $n = 3$ (or higher-lying states) at $t = \tau$, a quantum beat peak appears in the emission from np ($n \geq 3$) at intersections of the corresponding horizontal np emission line with the line B given by $\omega = E_{n=2} - E_{1s} + \omega_b$. Conversely, if the probe pulse transfers amplitude from $n = 3$ to $n = 2$, the peak at the same beat frequency appears in the emission from $2p$ at the intersection with the line B' with $\omega = E_{n=3} - E_{1s} - \omega_b$. Signatures of more complex paths involving higher-lying intermediate states are readily identified. For example, the interference between the paths $1s$ and $2p$ leaves its mark on the quantum beat spectrum of higher-lying states, e.g., $3p$ (line D with $\omega_b = E_{2p} - E_{1s}$).

In the low-frequency part of the quantum beat spectrum, a line-out of which is shown in Fig. 8, the peak in the emission from the $2p$ state near 1.89 eV contains contributions from the pair of paths involving the direct $2p$ path and one indirect path through the $3(s, p, d)$ state excited by the pump

pulse and deexcited to the $2p$ state by the probe pulse with an energy difference of $E_{3(s,p,d)} - E_{2p} = 1.89$ eV. Note that, because of the ℓ degeneracy, contributions from different ℓ states within the same n manifold cannot be distinguished. Analogously, the interference between the direct $2p$ path and an indirect path involving higher lying n states, e.g., $n = 4$ (s, p, d, f) or $n = 5$ (s, p, d, f, g) gives rise to peaks in the quantum beat spectrum at 2.55 and 2.85 eV (see Fig. 7). Furthermore, interference between two indirect paths reaching the $2p$ state at τ via excitation from the ground state to the $3(s, p, d)$ and to the $4(s, p, d, f)$ states by the pump pulse and subsequent transfer to the $2p$ state by the probe pulse gives rise to a peak corresponding to an energy difference of $E_{4(s,p,d,f)} - E_{3(s,p,d)} = 0.66$ eV, marked in Fig. 8(a). The high-frequency beat spectrum is shown in Fig. 9. This part of the beat spectrum results from interferences between those path pairs involving one path where the $2p$ state is reached from the ground state only through the probe pulse while the other is already excited by the pump pulse.

Conventional applications of quantum beat spectroscopy typically focus on optically allowed states. The present strong-field attosecond pump-probe quantum beat spectroscopy allows us to go beyond this limitation by accessing pairs of optically forbidden states due to multiphoton transitions driven by the OAS pulse. Moreover, it provides novel information on the nonlinear response of the electronic system in terms of the strength of the excitation [Eqs. (20) and (21)] and relative phases θ [Eq. (24)]. The relative height of the peaks is a direct measure for the strength of the coherent excitation of the interfering path pairs, i.e., the corresponding off-diagonal density matrix element ρ_{ij} . The height varies with the intensity of the pump pulse underlining the influence of nonlinear strong-field effects and shows that the beat signals offer the opportunity to probe the multiphoton transition strengths between excited states in spectral regions otherwise not directly accessible in the experiment.

The relative weight of the different pathways depends on an intricate interplay between the intensity and spectral distribution of the pump and probe pulses, the resulting transient excited-state coherences, and the emission strength. Taking the peak at $\omega_b = 1.89$ eV as an example, the transition from the $3(s, d)$ to $2p$ states by the probe pulse requires the emission of (at least) one photon, while the transition from the $3p$ state to the $2p$ state requires two photons. At first glance, this would suggest that the pathways [via $3(s, d)$] requiring only one-photon transitions induced by the weak probe pulse would dominate over the two-photon path (via $3p$). However, a detailed analysis shows a more complex pattern. As shown in Figs. 4 and 5, the population at the conclusion of the pump pulse may peak at $\ell = 1$. Moreover, the two-photon-induced transition from a higher-lying np state to the $2p$ state by the probe pulse may be enhanced by resonant intermediate states. Thus the two-photon transition strength may become comparable to or even larger than the one-photon transition strength for weak probe pulses.

The relative weight of the one- and two-photon transitions from the intermediate excited states to the $2p$ state can be controlled by the intensity of the probe pulse. By reducing the intensity of the probe pulse, the relative weight of all indirect paths to the $2p$ state, i.e., those by which the $2p$ state

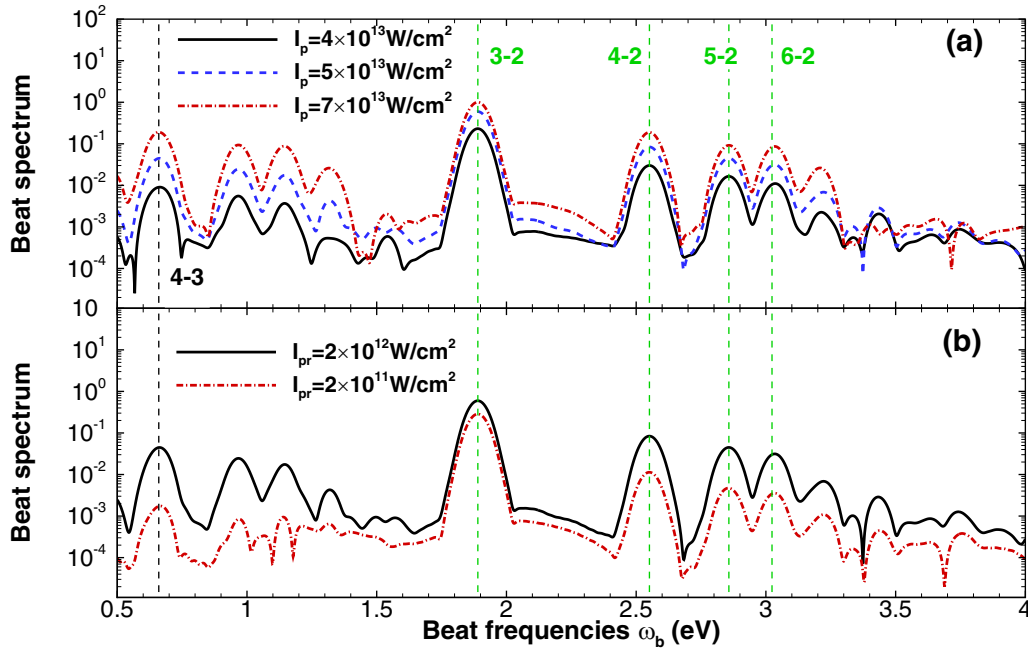


FIG. 8. (a) Quantum beat spectrum of the $2p$ emission line (10.20 eV) for three different intensities of the pump OAS pulse ($I_p = 4 \times 10^{13}$ W/cm 2 , 5×10^{13} W/cm 2 , and 7×10^{13} W/cm 2) and fixed probe intensity $I_{pr} = 2 \times 10^{12}$ W/cm 2 with a resolution $\sim 1/\tau$ of $\Delta E = 0.1$ eV, and (b) for different probe intensities ($I_{pr} = 2 \times 10^{12}$ W/cm 2 and 2×10^{11} W/cm 2) at a fixed pump intensity $I_p = 5 \times 10^{13}$ W/cm 2 . The quantum numbers of the coherently excited state pairs $n-n'$ contributing to the most prominent peaks are labeled.

is reached only during the probe pulse by a transition from an intermediate state, can be reduced, while, conversely, the direct path to the $2p$ state (the electron is already excited to the $2p$ state by the pump pulse, and it stays on the $2p$ state when the probe pulse passes) will be enhanced. The latter follows from the fact that the excited $2p$ level has a larger survival probability when the probe pulse is weaker.

The variation of the probe intensity by a factor 10 [Figs. 8(b) and 9(b)] results in significantly different heights of the beat peaks. This allows us to identify the relative importance of one- and two-photon transitions because the height of the beat peak is proportional to the product of the amplitudes of the two interfering quantum paths. Decreasing the probe intensity by a factor 10 implies for the

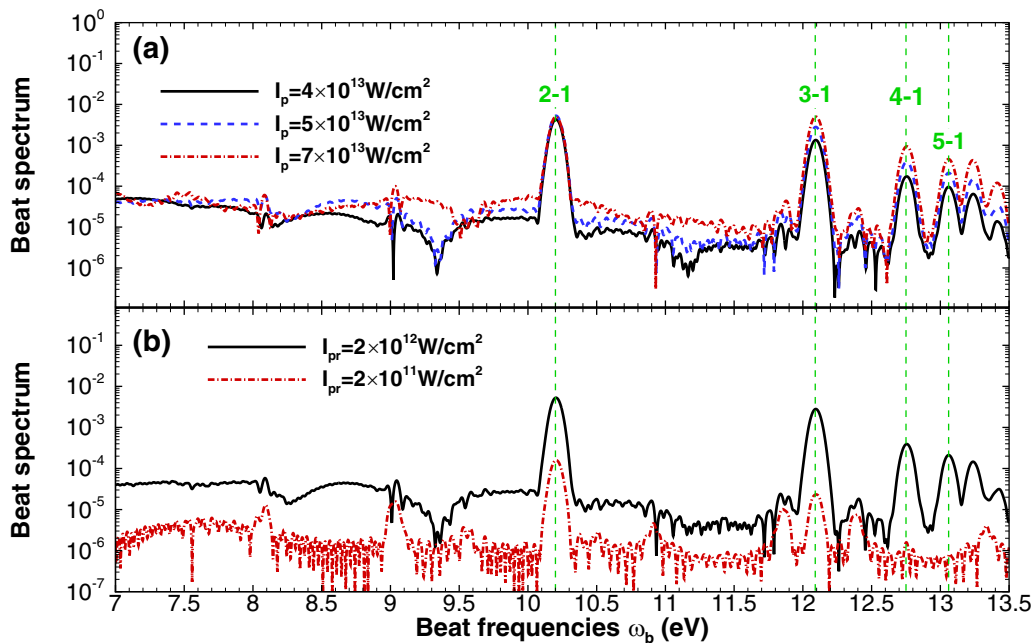


FIG. 9. The same as Fig. 8 but for the higher beat frequencies. The green labels denote the coherently excited state pairs (labeled by quantum numbers $n-n'$) contributing to the peaks.

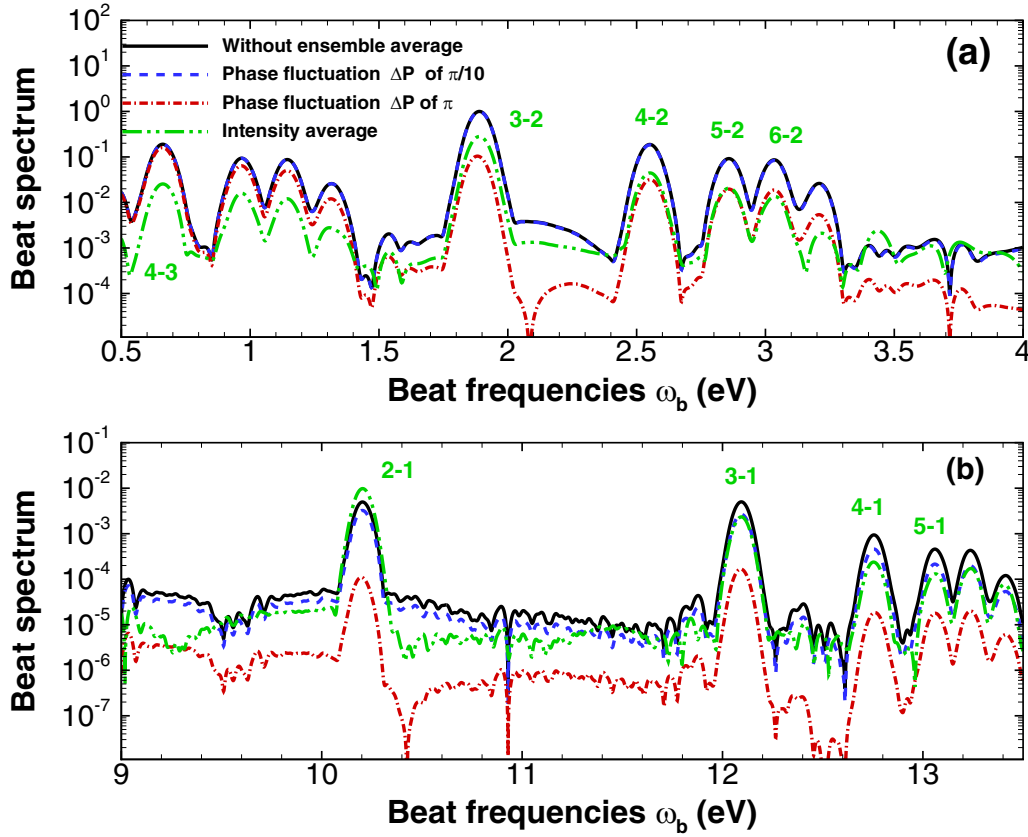


FIG. 10. (a) Same as Fig. 8 and (b) same as Fig. 9 but including decoherence due to intensity average over the focal volume or due to the phase fluctuations. The peak intensities of the pump pulse and the probe pulse are $I_p = 7 \times 10^{13}$ and $I_{pr} = 2 \times 10^{12}$ W/cm², respectively. The results without ensemble average (Figs. 8 and 9) are shown as reference. Phase fluctuations are simulated by assuming uniformly distributed random time delays between pump and probe corresponding to phase shifts $[-\pi/10, \pi/10]$ or $[-\pi, \pi]$. Intensity focal averaging over the pump field is performed for seven intensities from $I_p = 1 \times 10^{13}$ to $I_p = 7 \times 10^{13}$ W/cm² with the weights given in Refs. [44–46]. The green labels denote the coherently excited state pairs (labeled by n quantum numbers) contributing to the peaks.

amplitude of an indirect path a reduction by a factor $\sqrt{10}$ when the emitting state is reached by a one-photon transition while the reduction factor is 10 for a two-photon transition. For the beat peak 3-2 [see Fig. 8(b)], the reduction by ≈ 2.1 indicates that the one-photon transition can indeed be dominant. The fact that the ratio is even smaller than $\sqrt{10} \approx 3.16$ can be understood as a result of the relative enhancement of the direct path to $2p$ due to the increased survival probability. A dramatically different behavior is found for high-lying states where the ratio significantly exceeds $\sqrt{10}$ (e.g., 7.4 for $n = 4$) indicating a strong contribution from two-photon transitions in part mediated by near-resonant intermediate states.

We explore now the effects of decoherence due to ensemble average over different realizations of the OAS pulse on the quantum beat spectrum (see Fig. 10). We consider two prototypical scenarios: the inhomogeneous field distribution within the focal volume of the laser pulse and phase fluctuations which we simulate by assuming randomly distributed time delays between pump and probe centered around the nominal delay τ . We consider the case of random delays corresponding to small fluctuations with random phases $\Delta P \in [-\pi/10, \pi/10]$ and large fluctuations with random phases $\Delta P \in [-\pi, \pi]$. As expected, neither intensity variations nor phase fluctuations change the position of the peaks in the beat spectrum. While

the small phase fluctuations result only in a modest change of the peak heights, the large phase fluctuations lead to a significant overall reduction of the beat signal. Nevertheless, even in this limit, the pronounced quantum beat peaks survive.

Quantum beat spectroscopy gives direct access to the relative phases between different (de)excitation pathways of strong-field excitation and, thus, holographic information on the bound-state wave packet. Figure 11 displays the pump-pulse intensity dependence of the relative phases θ [Eq. (24)] of the path pairs $2p-3(s, p, d)$ and $2p-4(s, p, d)$ contributing to the quantum beats observed in the VUV emission from the $2p$ state. We observe strong phase variation of the coherence phases with the intensity of the pump pulse I_p and of the probe pulse I_{pr} reflecting the influence of subcycle dynamical Stark shifts and coupling to virtual intermediate states in the continuum. These large phase excursions with increasing OAS pump pulse strength reveal the high sensitivity of the phase response mapped out by the attosecond-pump attosecond-probe quantum beats. The observed coherence phases deviate strongly from the perturbative limit for lowest-order (multiphoton) transitions. For one- and two-photon transitions, the corresponding phases can be analytically estimated. One-photon transitions contribute (modulo π) a phase of $\pm\pi/2$. Two-photon transitions involving a resonant intermediate state

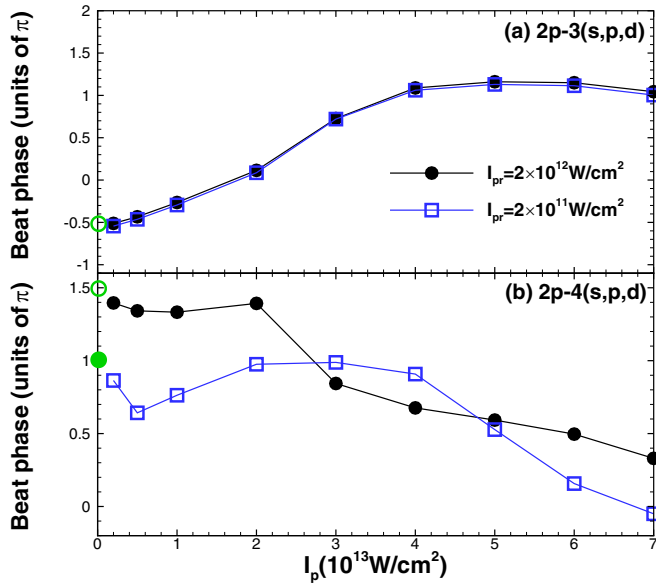


FIG. 11. The beat phase θ [Eq. (24)] as a function of the intensity of the pump pulse I_p for beat oscillations in the emission signal at beating frequencies corresponding to excitation of the path pairs (a) $[2p-3(s, d)]$ and (b) $[2p-4(s, p, d)]$. Results for two intensities of the probe pulse $I_{pr} = 2 \times 10^{12}$ W/cm 2 and 2×10^{11} W/cm 2 are shown. The perturbative lowest-order one- and two-photon transition phases are indicated by green circles near $I_p = 0$ in each panel.

yield 0, π , while in absence of such a resonance the phase contribution is $\pm\pi/2$. The probe intensity dependence is small for the $2p-3(s, p, d)$ pair but much more pronounced for the $2p-4(s, p, d)$ pair. This observation is consistent with the intensity dependence of the absolute height of the beat spectra shown in Fig. 8, indicating different numbers of photons involved in the deexcitation by the probe pulse as the probe pulse intensity changes.

V. CONCLUSIONS

In the present theoretical optical attosecond pump-probe study of bound-state quantum beats, we have demonstrated the novel opportunities for probing the nonlinear response and bound-state electronic wave packet motion in unprecedented detail. Interfering excitation paths involving multiphoton transitions and bound-state coherences can be unambiguously identified from the VUV emission signal. Strength and phase of a coherent excitation can be manipulated and controlled by the waveform of the optical attosecond pulse. The present study for atomic hydrogen can be readily generalized to rare-gas atoms. In particular, heavier rare-gas atoms (Kr, Xe, ...) for which the excitation gap Δ to the first-excited state is comparable to that of hydrogen, would be well suited. An experimental realization for Xe is planned [30]. Extension of the present approach to bound-state coherences created by HHG or or synchrotron-based pulses is straightforward [28]. Further applications to more complex systems such as polyatomic molecules and solids promise to generate predesigned coherent wave packets for both spectroscopic investigations of dipole-forbidden transitions and to trigger well-controlled rearrangement and charge migration.

ACKNOWLEDGMENTS

Stimulating discussions with E. Goulielmakis, M. Hassan, and S. Donsa are gratefully acknowledged. The present work was supported by Grants No. FWF-SFB049 (Nextlite), No. FWF-SFB041 (VICOM), No. WWTF MA1FOR-002, Doctoral college Grant No. FWF-W1243 (Solids4Fun), National Natural Science Foundation of China (No. 11804233 and No. 11747013). X.-M.T was supported by a Grant-in-aid for Scientific Research (Grant No. JP16K05495) from the Japan Society for the Promotion of Science. Part of the calculation was performed using the COMA, Oakforest-Pac supercomputers at the Center for Computational Science, University of Tsukuba, and VSC 3 Vienna.

APPENDIX A: LIOUVILLE SPACE AND SUPEROPERATOR NOTATION

The theory of quantum-beat spectroscopy can be concisely formulated with the help of the superoperator formalism in Liouville space used in the main text. For completeness and clarity we briefly review here definitions of its key elements. A more detailed discussion can be found in, e.g., in Refs. [39–41,43]. Accordingly, a Hilbert-space operator A expressed in the Hilbert-space basis $\{|i\rangle\}$,

$$A = \sum_{i,j} |i\rangle A_{ij} \langle j|, \quad (\text{A1})$$

becomes a Liouville state (or Liouville ket) in Liouville space,

$$|A\rangle = A, \quad (\text{A2})$$

where rounded kets are used to distinguish Liouville kets from kets in Hilbert space. If the operator A is represented by a matrix in an N -dimensional subspace of the Hilbert space, the corresponding Liouville subspace representation possesses dimension N^2 . The scalar product (or Liouville bracket) between two Liouville kets $|A\rangle$ and $|B\rangle$ is given in terms of the trace

$$\langle A|B\rangle = \text{Tr}(A^+B) = \sum_{ij} A_{ji}^* B_{ji}. \quad (\text{A3})$$

The induced norm $\| |A\rangle \|^2 = \langle A|A\rangle$ corresponds to the Hilbert-Schmidt norm for matrices. The trace of an operator, $\text{Tr}(A)$ can be expressed as a Liouville bracket

$$\langle \mathbb{I}|A\rangle = \text{Tr}A, \quad (\text{A4})$$

with

$$|\mathbb{I}\rangle = \sum_i |i\rangle \langle i| \quad (\text{A5})$$

being the unit vector in Liouville space. A unitary transformation of A is represented by a superoperator \mathcal{U} :

$$\mathcal{U}|A\rangle = UAU^+, \quad (\text{A6})$$

with U being the corresponding transformation operator in Hilbert space. In particular, the differential change $\Delta|\rho\rangle$ of the density operator under infinitesimal time translation in Liouville space is given by

$$i\Delta|\rho\rangle = \mathcal{L}|\rho\rangle\Delta t, \quad (\text{A7})$$

or

$$i\frac{\partial}{\partial t}|\rho\rangle = \mathcal{L}|\rho\rangle, \quad (\text{A8})$$

with

$$\mathcal{L}|\rho\rangle = [H, \rho], \quad (\text{A9})$$

where H is the Hamiltonian operator in Hilbert space, \mathcal{L} the Liouvillian operator in Liouville space, and

$$|\rho\rangle = \sum_{i,j} \rho_{ij} |i\rangle\langle j|. \quad (\text{A10})$$

In matrix form, Eq. (A9) explicitly reads

$$[\mathcal{L}|\rho\rangle]_{i,j} = \sum_{i',j'} \mathcal{L}_{j,j'}^{i,i'} \rho_{i',j'}, \quad (\text{A11})$$

with

$$\mathcal{L}_{j,j'}^{i,i'} = H_{i,i'} \delta_{j,j'} - H_{j,j} \delta_{i,i'}. \quad (\text{A12})$$

Correspondingly, the time evolution from time t_0 to time t_1 reads

$$|\rho(t_1)\rangle = \mathcal{U}(t_1, t_0) |\rho(t_0)\rangle, \quad (\text{A13})$$

with

$$\mathcal{U}(t_1, t_0) = \hat{T} \exp\left(-i \int_{t_0}^{t_1} \mathcal{L}(t') dt'\right), \quad (\text{A14})$$

and \hat{T} being the time-ordering operator. Equation (A8) is employed in the main text to describe and analyze the time evolution of $|\rho(t)\rangle$ during the pump-probe sequence of optical attosecond pulses.

APPENDIX B: QUANTUM BEATS IN SPONTANEOUS EMISSION

We briefly summarize the theory of quantum beats observed in the spontaneous photon emission signal emitted from coherently excited atomic states $\{|i\rangle\}$. The starting point is the Wigner-Weisskopf approximation [47,48] for decay of excited states by spontaneous emission of photons due to coupling to vacuum fluctuations of the quantized radiation field

$$|i(t)\rangle = |i(0)\rangle \exp[-i(E_i - i\Gamma_i/2)t], \quad (\text{B1})$$

with E_i the energy and Γ_i the homogeneous linewidth (or $\tau_i = \Gamma_i^{-1}$ its radiative lifetime). Equation (B1) describes the time evolution of a state excited at time $t = 0$. (In the main text, the starting time of the field-free evolution and decay is shifted to $t = \tau + \Delta_{\text{pr}}$ when the probe pulse has concluded).

The multidifferential rate for spontaneous emission of photons with energy ω_k into direction \hat{k} at time t is given in dipole approximation by [39,54,55]

$$S_s(\hat{k}, \omega_k, t) = \frac{\omega_k}{4\pi^2 c^3} \sum_{i,j,f} \sum_{\alpha} \langle f | \hat{e}_{\hat{k},\alpha} \cdot \mathbf{p} | i \rangle \cdot \langle f | \hat{e}_{\hat{k},\alpha} \cdot \mathbf{p} | j \rangle^* G(t) \rho_{i,j}(0), \quad (\text{B2})$$

where $\rho_{i,j}(0)$ denotes the excited-states density matrix in the energy basis, α the polarization index of the emitted photon and $G(t)$ the propagator in the absence of external

electromagnetic fields. $G(t)$ is explicitly given by

$$G(t) = \exp[i(E_f + \omega_k - E_i)t + (\Gamma_f - \Gamma_i)t/2] \times \frac{\exp[-i(E_f + \omega_k - E_j)t + (\Gamma_f - \Gamma_j)t/2] - 1}{\omega_k + E_f - E_j + i(\Gamma_f - \Gamma_j)/2} + \exp[i(E_f + \omega_k - E_j)t + (\Gamma_f - \Gamma_j)t/2] \times \frac{\exp[-i(E_f + \omega_k - E_i)t + (\Gamma_f - \Gamma_i)t/2] - 1}{\omega_k + E_f - E_i + i(\Gamma_f - \Gamma_i)/2}. \quad (\text{B3})$$

$G(t)$ is strongly peaked near the transition energies $\omega_k = E_i - E_f$ and $\omega_k = E_j - E_f$ for a time-resolved measurement with a time resolution Δt corresponding to a Fourier width

$$\Delta\omega_k = \frac{1}{\Delta t}. \quad (\text{B4})$$

In the following, $\Delta\omega_k$ is assumed to be large compared with the natural linewidths ($\Gamma_f, \Gamma_i, \Gamma_j$) but small compared with the transition energies $|E_i - E_f|, |E_j - E_f|$. The rate for spontaneous emission into the spectral window $[\bar{\omega}_k \pm \Delta\omega_k/2]$ is

$$S_s(\hat{k}, \bar{\omega}_k, t) = \int_{\bar{\omega}_k - \Delta\omega_k/2}^{\bar{\omega}_k + \Delta\omega_k/2} d\omega_k S_s(\hat{k}, \omega_k, t). \quad (\text{B5})$$

Equation (B5) can be evaluated by complex contour integration after extending the integration limit from $-\infty$ to $+\infty$ with negligible error yielding the time-differential spontaneous emission rate

$$S_s(\hat{k}, \bar{\omega}_k, t) = \frac{\bar{\omega}_k}{2\pi c^3} \sum_{i,j,f} \sum_{\alpha} \langle f | \hat{e}_{\hat{k},\alpha} \cdot \mathbf{p} | i \rangle \langle f | \hat{e}_{\hat{k},\alpha} \cdot \mathbf{p} | j \rangle^* \times \rho_{i,j}(0) \exp[i(E_j - E_i)t - (\Gamma_i + \Gamma_j)t/2]. \quad (\text{B6})$$

In Eq. (B6) the sum over states \sum' is truncated to those combinations $\{i, j, f\}_{\bar{\omega}_k}$ of state pairs whose transition energies $|E_i - E_f|, |E_j - E_f|$ lie within the unresolved spectral window $[\bar{\omega}_k \pm \Delta\omega_k/2]$. Throughout the main text, we use a Gaussian rather than a rectangular spectral window function with FWHM $\Delta\omega_k$. Equation (B6) represents the quantum beats in the time-differential emission rate when the spectral window contains more than one initial state with $E_i \neq E_j$. It should be noted that $S_s(\hat{k}, \bar{\omega}_k, t)$ simultaneously features a coarse-grained dependence on both the time t and the transition energy $\bar{\omega}_k$. It allows resolution of quantum beats with frequencies $E_i - E_j$ due to path interferences between spontaneous decay paths $i \rightarrow f$ and $j \rightarrow f$ provided that both transition energies lie within the spectral window $[\bar{\omega}_k \pm \Delta\omega_k/2]$. At the same time it selects photon energies near $\bar{\omega}_k$ within the bandwidth $\Delta\omega_k$.

Integration over all emission directions \hat{k} and summation over the polarizations yields the total spontaneous rate

$$S_s(\bar{\omega}_k, t) = \frac{4\bar{\omega}_k}{3c^3} \sum_{i,j,f} \langle f | \mathbf{p} | i \rangle \langle f | \mathbf{p} | j \rangle^* \times \rho_{i,j}(0) \exp[i(E_j - E_i)t - (\Gamma_i + \Gamma_j)t/2]. \quad (\text{B7})$$

In the special case of the transition from a single level, e.g., the Lyman $2p \rightarrow 1s$ transition,

$$S_s(\bar{\omega}_k, \tau, t) = \frac{4\bar{\omega}_k}{3c^3} |\langle f | \mathbf{p} | i \rangle|^2 \exp(-\Gamma_i t) \rho_{i,i}(0). \quad (\text{B8})$$

In acceleration gauge used in the main text, Eq. (B8) becomes

$$S_s(\bar{\omega}_k, \tau, t) = \frac{4}{3c^3 \bar{\omega}_k} |\langle f | \mathbf{p} | i \rangle|^2 \exp(-\Gamma_i t) \rho_{i,i}(0). \quad (\text{B9})$$

Note that in the main text the state undergoing radiative decay is labeled by $|e\rangle$ instead of $|i\rangle$. Quantum beat due to interferences between different spontaneous decay paths are absent in the case of Eq. (B8). However, beats can still be observed that are encoded in the initial diagonal density-matrix element $\rho_{i,i}(0)$ as a result of a preceding pump-probe sequence as discussed in the main text. In this case, these beats

appear also in the time-integral signal

$$\begin{aligned} S_s(\bar{\omega}_k) &= \int_0^\infty dt S_s(\bar{\omega}_k, t) \\ &= \frac{4}{3c^3 \Gamma_i \bar{\omega}_k} |\langle f | \mathbf{a} | i \rangle|^2 \rho_{i,i}(0). \end{aligned} \quad (\text{B10})$$

If $|f\rangle$ is the only radiative decay channel of the state $|i\rangle$,

$$S_s(\bar{\omega}_k) = \rho_{i,i}(0), \quad (\text{B11})$$

since in this case

$$\Gamma_i = \frac{4}{3c^3 \bar{\omega}_k} |\langle f | \mathbf{a} | i \rangle|^2. \quad (\text{B12})$$

Quantum beats due to interference between different spontaneous paths appear only in the time-differential emission [Eq. (B7)]. In the present case discussed in the main text these beats appear at smaller $\bar{\omega}_k$ matching transition energies $n \rightarrow n'$ ($n, n' \geq 2$) (not shown in the main text).

-
- [1] F. Krausz and M. Ivanov, *Rev. Mod. Phys.* **81**, 163 (2009).
 [2] T. Weinacht, J. Ahn, and P. Bucksbaum, *Nature (London)* **397**, 233 (1999).
 [3] P. B. Corkum and F. Krausz, *Nat. Phys.* **3**, 381 (2007).
 [4] P. Johnsson, J. Mauritsson, T. Remetter, A. L'Huillier, and K. J. Schafer, *Phys. Rev. Lett.* **99**, 233001 (2007).
 [5] M. Lucchini, A. Ludwig, T. Zimmermann, L. Kasmi, J. Herrmann, A. Scrinzi, A. S. Landsman, L. Gallmann, and U. Keller, *Phys. Rev. A* **91**, 063406 (2015).
 [6] R. Pazourek, S. Nagele, and J. Burgdörfer, *Rev. Mod. Phys.* **87**, 765 (2015).
 [7] E. Constant, V. D. Taranukhin, A. Stolow, and P. B. Corkum, *Phys. Rev. A* **56**, 3870 (1997).
 [8] J. Itatani, F. Quéré, G. L. Yudin, M. Y. Ivanov, F. Krausz, and P. B. Corkum, *Phys. Rev. Lett.* **88**, 173903 (2002).
 [9] V. Vénier, R. Taïeb, and A. Maquet, *Phys. Rev. A* **54**, 721 (1996).
 [10] K. Klünder *et al.*, *Phys. Rev. Lett.* **106**, 143002 (2011).
 [11] C. Leichtle, W. P. Schleich, I. S. Averbukh, and M. Shapiro, *Phys. Rev. Lett.* **80**, 1418 (1998).
 [12] J. Mauritsson, T. Remetter, M. Swoboda, K. Klünder, A. L'Huillier, K. J. Schafer, O. Ghafur, F. Kelkensberg, W. Siu, P. Johnsson *et al.*, *Phys. Rev. Lett.* **105**, 053001 (2010).
 [13] E. Goulielmakis *et al.*, *Nature (London)* **466**, 739 (2010).
 [14] R. Santra, V. S. Yakovlev, T. Pfeifer, and Z.-H. Loh, *Phys. Rev. A* **83**, 033405 (2011).
 [15] S. Bashkin (Ed.), *Beam-foil spectroscopy* (Gordon and Breach, New York, 1968).
 [16] S. Bashkin, *Appl. Opt.* **7**, 2341 (1968).
 [17] H. J. Andrä, *Phys. Rev. Lett.* **25**, 325 (1970).
 [18] H. J. Andrä, *Phys. Rev. A* **2**, 2200 (1970).
 [19] H. Schröder, *Z. Phys. A: At. Nucl.* (1975) **284**, 125 (1978).
 [20] I. A. Sellin, L. Liljeby, S. Mannervik, and S. Hultberg, *Phys. Rev. Lett.* **42**, 570 (1979).
 [21] J. Burgdörfer, *Phys. Rev. Lett.* **43**, 505 (1979).
 [22] A. H. Zewail, *Femtochemistry: Ultrafast Dynamics of the Chemical Bond*, World Scientific Series in 20th Century Chemistry (World Scientific, 1994), Vol. 3.
 [23] A. H. Zewail, *J. Phys. Chem. A* **104**, 5660 (2000).
 [24] R. Pazourek, M. Reduzzi, P. A. Carpeggiani, G. Sansone, M. Gaarde, and K. Schafer, *Phys. Rev. A* **93**, 023420 (2016).
 [25] S. X. Hu and L. A. Collins, *Phys. Rev. Lett.* **96**, 073004 (2006).
 [26] I. Lontos *et al.*, *Opt. Lett.* **35**, 832 (2010).
 [27] D. Z. Kandula, C. Gohle, T. J. Pinkert, W. Ubachs, and K. S. E. Eikema, *Phys. Rev. A* **84**, 062512 (2011).
 [28] Y. Hikosaka, T. Kaneyasu, M. Fujimoto, H. Iwayama, and M. Katoh, *Nat. Commun.* **10**, 4988 (2019).
 [29] M. T. Hassan *et al.*, *Nature (London)* **530**, 66 (2016).
 [30] E. Goulielmakis *et al.* (private communication).
 [31] M. Lewenstein, P. Balcou, M. Y. Ivanov, A. L'Huillier, and P. B. Corkum, *Phys. Rev. A* **49**, 2117 (1994).
 [32] M. Ferray *et al.*, *J. Phys. B: At., Mol. Opt. Phys.* **21**, L31 (1988).
 [33] A. McPherson *et al.*, *J. Opt. Soc. Am. B* **4**, 595 (1987).
 [34] S. Bengtsson *et al.*, *Nat. Photonics* **11**, 252 (2017).
 [35] W. Cao, E. R. Warrick, A. Fidler, D. M. Neumark, and S. R. Leone, *Phys. Rev. A* **94**, 053846 (2016).
 [36] S. Beaulieu, E. Bloch, L. Barreau, A. Comby, D. Descamps, R. Généaux, F. Légaré, S. Petit, and Y. Mairesse, *Phys. Rev. A* **95**, 041401(R) (2017).
 [37] S. Beaulieu *et al.*, *Phys. Rev. Lett.* **117**, 203001 (2016).
 [38] H. Yun *et al.*, *Nat. Photon.* **12**, 620 (2018).
 [39] K. Blum, *Density Matrix Theory and Applications* (Springer-Verlag, 1981).
 [40] H. Gabriel, *Phys. Rev.* **181**, 506 (1969).
 [41] J. Bosse and H. Gabriel, *Eur. Phys. J. A* **266**, 283 (1974).
 [42] H. J. Andrä, *Phys. Scr.* **9**, 257 (1974).
 [43] U. Fano, *Phys. Rev.* **131**, 259 (1963).
 [44] G. N. Gibson, R. R. Freeman, T. J. McIlrath, and H. G. Muller, *Phys. Rev. A* **49**, 3870 (1994).
 [45] M. A. Walker, P. Hansch, and L. D. Van Woerkom, *Phys. Rev. A* **57**, R701 (1998).
 [46] S. Augst, D. D. Meyerhofer, D. P. Strickland, and S. L. Chin, *J. Opt. Soc. Am. B* **8**, 858 (1991).
 [47] V. Weisskopf and E. Wigner, *Eur. Phys. J. A* **63**, 54 (1930).

- [48] V. Weisskopf and E. Wigner, *Eur. Phys. J. A* **65**, 18 (1930).
- [49] W.-C. Jiang and X.-Q. Tian, *Opt. Express* **25**, 26832 (2017).
- [50] T. N. Rescigno and C. W. McCurdy, *Phys. Rev. A* **62**, 032706 (2000).
- [51] M. J. Rayson, *Phys. Rev. E* **76**, 026704 (2007).
- [52] B. I. Schneider and L. A. Collins, *J. Non-Cryst. Solids* **351**, 1551 (2005).
- [53] V. Stooß, S. M. Cavaletto, S. Donsa, A. Blättermann, P. Birk, C. H. Keitel, I. Březinová, J. Burgdörfer, C. Ott, and T. Pfeifer, *Phys. Rev. Lett.* **121**, 173005 (2018).
- [54] J. Barrat and C. Cohen-Tannoudji, *J. Phys. (Paris)* **22**, 329 (1961).
- [55] J. Burgdörfer, Ph.D. thesis, Free University Berlin, 1981 (unpublished).